Mitochondrial and cytosolic thiol redox state are not detectably altered in isolated human NADH:ubiquinone oxidoreductase deficiency

Sjoerd Verkaart [a,b,d,e], Werner J.H. Koopman [a,c,d], Julia Cheek [a,d], Sjenet E. van Emst-de Vries [a,d], Lambertus W.P.J. van den Heuvel [b,d,e], Jan A.M. Smeitink [b,d,e,*], Peter H.G.M. Willems [a,c,d]

[a] Department of Membrane Biochemistry, Radboud University Nijmegen Medical Centre, Nijmegen, The Netherlands
[b] Department of Pediatrics, Radboud University Nijmegen Medical Centre, Nijmegen, The Netherlands
[c] Microscopical Imaging Centre, Radboud University Nijmegen Medical Centre, Nijmegen, The Netherlands
[d] Nijmegen Centre for Molecular Life Sciences (NCMLS), Radboud University Nijmegen Medical Centre, Nijmegen, The Netherlands
[e] Nijmegen Centre for Mitochondrial Disorders (NCMD), Department of Pediatrics, Radboud University Nijmegen Medical Centre, P.O. Box 9101, 6500 HB Nijmegen, The Netherlands

Abstract

Isolated complex I deficiency is the most common enzymatic defect of the oxidative phosphorylation (OXPHOS) system, causing a wide range of clinical phenotypes. We reported before that the rates at which reactive oxygen species (ROS)-sensitive dyes are converted into their fluorescent oxidation products are markedly increased in cultured skin fibroblasts of patients with nuclear-inherited isolated complex I deficiency. Using video-imaging microscopy we show here that these cells also display a marked increase in NAD(P)H autofluorescence. Linear regression analysis revealed a negative correlation with the residual complex I activity and a positive correlation with the oxidation rates of the ROS-sensitive dyes 5-(and-6)-chloromethyl-2′,7′-dichlorodihydrofluorescein and hydroethidine for a cohort of 10 patient cell lines. On the other hand, video-imaging microscopy of cells expressing reduction–oxidation sensitive GFP1 in either the mitochondrial matrix or cytosol showed the absence of any detectable change in thiol redox state. In agreement with this result, neither the glutathione nor the glutathione disulfide content differed significantly between patient and healthy fibroblasts. Finally, video-rate confocal microscopy of cells loaded with C11-BODIPY$^{581/591}$ demonstrated that the extent of lipid peroxidation, which is regarded as a measure of oxidative damage, was not altered in patient fibroblasts. Our results indicate that fibroblasts of patients with isolated complex I deficiency maintain their thiol redox state despite marked increases in ROS production.

1. Introduction

NADH:ubiquinone oxidoreductase or complex I (EC 1.6.5.3.) is the main entry point of metabolic electrons into the oxidative phosphorylation (OXPHOS) ATP system and its proper function is essential for the adequate production of ATP. In accordance with this function, defects in complex I have been found to be associated with a wide range of human disorders including early onset, fatal clinical phenotypes such as Leigh and Leigh-like syndrome, encephalomyopathy and cardiomyopathy [1]. In mammals, the complex consists of 38 nuclear-

encoded and seven mitochondrial-encoded subunits, together having a molecular weight close to 1 MDa [2–4]. As far as the nuclear genome is concerned, disease-causing mutations have been identified in nine complex I subunits [5–8] and the complex I assembly factor B17.2L [9].

At the cellular level, these mutations were shown to decrease the amount of catalytically active complex [10]. Live cell studies revealed that the consequent decrease in NADH-oxidizing capacity was associated with altered mitochondrial morphology [11], disturbed Ca^{2+} and ATP handling [12,13] and increased rates of ROS production [14–16].

In healthy cells, the large majority of ROS are generated as a consequence of oxidative phosphorylation [17,18]. OXPHOS-derived ROS levels, carefully balanced by ROS scavenging systems, have been suggested to play an important signaling role in gearing mitochondrial and cellular physiology for one another [19,20]. Most probably, ROS act through promoting the reversible S-glutathionylation of regulatory proteins by glutathione S-transferases [21]. Evidence has been provided that OXPHOS-derived ROS predominantly originate from reduced flavin in complex I [22]. The fraction of reduced flavin was found to depend on the ratio and concentrations of NADH and NAD^+, thus explaining previous findings that NADH to NAD^+ ratio and ROS production are closely correlated [23–27]. Increased ROS production, as observed in cultured cells of complex I deficient patients (see above), may result in a condition of oxidative stress that, if persistent, may lead to cellular injury and, eventually, death [28,29].

The cell's redox environment is crucial in integrating multiple metabolic, signaling and transcriptional processes [30]. Because of the high intracellular glutathione concentration (1–11 mM), the glutathione disulfide (GSSG)–glutathione (GSH) redox couple is widely believed to be the major determinant of the cell's redox environment [31,32]. GSH can react nonenzymatically with ROS or function as a substrate for glutathione peroxidases and glutathione S-transferases [32,33]. Glutathione peroxidases catalyze the conversion of H_2O_2 to water, whereas glutathione S-transferases reversibly S-glutathionylate proteins to buffer excess ROS production [21]. Moreover, these transferases conjugate GSH with toxic products from lipid peroxidation such as 4-hydroxynonenal [34]. GSH is synthesized in the cytosol, from where it is imported into the mitochondrial matrix [35]. A number of studies have implicated the mitochondrial GSH pool in the loss of cell viability evoked by cellular GSH depletion [36,37]. Recent work demonstrated an increased sensitivity of mitochondrial GSH-depleted cells to peroxynitrite-induced damage [38]. In other studies, induction of mitochondrial oxidative stress was shown to decrease the mitochondrial GSH pool and to increase membrane lipid peroxidation [34].

Here, we provide evidence that the subcellular redox environment is not detectably altered in cultured skin fibroblasts of patients with nuclear-inherited isolated complex I deficiency. In agreement with this result, no significant changes in lipid peroxidation were observed.

2. Materials and methods

2.1. Patient skin fibroblasts

Fibroblasts were derived from skin biopsies of ten patients in the age range of 0–5 years (P1–P10) in whom an isolated NADH:ubiquinone oxidoreductase deficiency was confirmed in both muscle tissue and cultured fibroblasts and ten healthy control subjects, five adults (CT1–CT5) and five age-matched children (CT6–CT10), following informed consent and according to relevant institutional review boards (Table 1). Genetic characterization revealed disease-causing mutations in either the *NDUFV1* (P1–P2), *NDUFS1* (P3), *NDUFS2* (P4–P5), *NDUFS4* (P6–P8), *NDUFS7* (P9) or *NDUFS8* (P10) gene of complex I [7]. None of the patients harbored mitochondrial DNA mutations previously associated with CI deficiency. Measurement of complex I activity was performed in a mitochondria-enriched fraction obtained from cultured skin fibroblasts as described previously [39]. The activity of the complex was normalized against that of complex IV (cytochrome *c* oxidase), which was measured in the same fraction, and expressed as percentage of lowest control (110 mU/U cytochrome *c* oxidase; [39]). Fibroblasts were cultured in medium 199 with Earle's salt supplemented with 10% (v/v) fetal calf serum, 100 IU/ml penicillin and 100 IU/ml streptomycin in a humidified atmosphere of 95% air and 5% CO_2 at 37 °C. Initial passage numbers are given in Verkaart et al. [15] and measurements were performed within 5 passages. Cell cycle analysis revealed no differences between the various cell lines [11].

2.2. Quantification of intracellular NAD(P)H autofluorescence

For measurement of intracellular NAD(P)H autofluorescence, fibroblasts were seeded on glass coverslips (Ø24 mm) and cultured to ~70% confluence. Immediately prior to measurement, cells were transferred to a HEPES–Tris medium (132 mM NaCl, 4.2 mM KCl, 1 mM $CaCl_2$, 1 mM $MgCl_2$, 5.5 mM D-glucose and 10 mM HEPES, pH 7.4) and coverslips were mounted in an incubation chamber placed on the stage of an inverted microscope (Axiovert 200 M, Carl Zeiss, Jena, Germany) equipped with a Zeiss 40×/1.3 NA Plan NeoFluar objective. The cells were excited at 360 nm using a monochromator (Polychrome IV, TILL Photonics, Gräfelfing, Germany). Fluorescence emission light was directed by a 415DCLP dichroic mirror (Omega Optical Inc., Brattleboro, VT, USA) through a 510WB40 emission filter (Omega Optical Inc.) onto a CoolSNAP HQ monochrome CCD-camera (Roper Scientific, Vianen, The Netherlands). The imaging setup was controlled by Metafluor 6.0 software (Universal Imaging Corporation, Downingtown, PA, USA). Routinely, 10 fields of view were analyzed per coverslip using an image capturing time of 100 ms. The mean fluorescence intensity was determined in an intracellular region of interest and, for purpose of background correction, an extracellular region of identical size. Quantitative image analysis was performed with Metamorph 6.0 (Universal Imaging Corporation). In each experiment, the average value obtained with healthy fibroblasts was set at 100%, to which all other values were related.

2.3. Quantification of hydroethidine and CM-H₂DCF oxidation

Quantitative determination of fluorescent oxidation products of hydroethidine (HEt) and (5-(and-6)-chloromethyl-2′,7′-dichlorodihydrofluorescein (CM-H₂DCF) was performed as described previously [15,40,41]. Briefly, fibroblasts, grown to ~70% confluence on glass coverslips, were incubated in HEPES–Tris medium containing either 10 μM HEt or 1 μM CM-H₂DCFDA for 10 min at 37 °C. After thorough washing to remove non-oxidized HEt or non-hydrolyzed CM-H₂DCFDA, coverslips were mounted in an incubation chamber placed on the stage of either the video-imaging microscope or a confocal microscope (Noran Instruments, Middleton, WI, USA). Initial measurements revealed that the formation of fluorescent oxidation products occurred linearly with time during both the incubation period in the presence of HEt (data not shown) and the imaging period in the presence of CM-H₂DCF [41], indicating a zero-order reaction mechanism. This means that in both cases the rate of fluorescence increase is a measure of the level of the oxidant that oxidizes the dye. HEt is thought to be primarily oxidized by superoxide, whereas superoxide-derived ROS are

Table 1
NADH(P)H autofluorescence, oxidation of ROS-sensitive dyes and extent of lipid peroxidation

Cell line [a]	Affected subunit and mutation [b]	CI activity [c]	NAD(P)H auto-fluorescence	Rate of HEt oxidation [d]	Rate of CM-H$_2$DCF oxidation [d]	C11-BODIPY[581/591] fluorescence emission ratio [e]
Average CT		106±2.4	98.3±6.69	100±0.66	108±8.33	115±10
CT1 (#5120)	None	113	100±2 (n=143)	100±1 (n=526)	100±2 (n=412)	100±3 (n=99)
CT2 (#5119)	None	105	86±2 (n=101)	102±2 (n=89)	100±11 (n=48)	135±5 (n=112)
CT3 (#5118)	None	103	109±3 (n=94)	98±3 (n=126)	125±13 (n=61)	110±4 (n=108)
CT4 (#4996)	None	n.d.	n.d.	100±3 (n=95)	n.d.	n.d.
CT5 (#223V)	None	103	n.d.	99±3 (n=94)	n.d.	n.d.
Average P		49±6.3	142±7.23	181±14.0	223±20.8	112±4
P1 (#5171)	NDUFV1-R59X/T423M	**73**	**130±9 (n=18)**	**186±6 (n=84)**	**242±19 (n=78)**	92±3 (n=73)
P2 (#5866)	NDUFV1-R59X/T423M	**64**	**142±4 (n=93)**	110±3 (n=61)	**135±12 (n=49)**	123±3 (n=108)
P3 (#6173)	NDUFS1-D618N/R577X	**31**	**142±5 (n=60)**	**176±4 (n=83)**	**171±13 (n=87)**	109±3 (n=74)
P4 (#5170)	NDUFS2-R228Q	**39**	**140±7 (n=61)**	**205±8 (n=66)**	**169±7 (n=124)**	115±4 (n=101)
P5 (#5067)	NDUFS2-P229Q	**36**	**191±6 (n=102)**	**264±9 (n=100)**	**351±41 (n=28)**	115±5 (n=64)
P6 (#5260)	NDUFS4-R106X	**36**	**132±4 (n=114)**	**174±8 (n=64)**	**187±12 (n=160)**	127±4 (n=64)
P7 (#5737)	NDUFS4-VPEEHI67/VEKSIstop	**53**	**127±6 (n=70)**	**131±4 (n=92)**	**202±12 (n=98)**	115±4 (n=81)
P8 (#4608)	NDUFS4-K158fs	**75**	**130±4 (n=62)**	**195±6 (n=106)**	**289±46 (n=29)**	123±5 (n=76)
P9 (#5175)	NDUFS7-V122M	**68**	112±7 (n=40)	**151±5 (n=94)**	**212±15 (n=76)**	87±3 (n=99)
P10 (#6603)	NDUFS8-R94C	**18**	**170±6 (n=62)**	**222±7 (n=147)**	**275±20 (n=117)**	111±3 (n=90)

Statistics: values in bold are below the lowest control value (CI activity) or significantly different ($p<0.05$) from highest control (NAD(P)H autofluorescence, rate of HEt oxidation, rate of CM-H$_2$DCF oxidation). Values between brackets represent the number of individual cells analyzed on at least 2 days.

[a] Numbers indicate the designation of the cell lines within the Nijmegen Centre for Mitochondrial Disorders (NCMD). CT and P indicate control and patient cell lines, respectively.

[b] Mutations are given at the protein level.

[c] Enzymatic activities were measured in mitochondria-enriched fractions and expressed as % of the lowest control value (110 mU/U cytochrome c oxidase).

[d] Determined previously and expressed as % of CT1 [15,16].

[e] Expressed as % of CT1.

thought to predominantly oxidize CM-H$_2$DCF. In each experiment, the average value obtained with healthy fibroblasts was set at 100%, to which all other values were related.

2.4. Quantification of cytosolic and mitochondrial thiol redox state

cDNA's encoding roGFP1 and mitochondria-targeted roGFP1 [42,43] were digested from a pEGFP-N1 vector backbone using *Eco*RI/*Xba*I and *Nde*I/*Xba*I, respectively. For expression in mammalian cells, inserts were ligated into a modified pFastbacdual transfer vector [12]. RoGFP1 contains surface-exposed cysteine residues that form disulfide bonds upon oxidation. The fluorescence emission ratio after excitation at 400 nm (oxidized state) and 480 nm (reduced state) is a measure of the ambient redox potential [42,43]. The ratiometric nature of the probe minimizes errors associated with changes in roGFP1 expression, photobleaching, and variations in cell thickness [43]. Moreover, roGFP1 fluorescence is pH-independent, which allows comparison of roGFP1 signals between the cytosolic and the more alkaline mitochondrial matrix [17]. For roGFP1 experiments, human skin fibroblasts, seeded on glass coverslips (Ø 24 mm), were cultured for 24 h, infected with the appropriate baculovirus and cultured for another 48 h. Immediately prior to fluorescence measurement, fibroblasts were transferred to HEPES–Tris medium and coverslips were mounted in an incubation chamber placed on the stage of the video-imaging microscope. RoGFP1 was alternately excited at 400 and 480 nm using the monochromator and fluorescence emission light was directed by a 525DRLP dichroic mirror (Omega Optical Inc.) through a 535DF25 emission filter (Omega Optical Inc.) onto the CCD-camera. Image capturing time was 300 ms and a pair of images was taken every 5 s. For each wavelength, the mean fluorescence intensity was monitored in an intracellular region and, for purpose of background correction, an extracellular region of identical size. After equilibration for 3 min, cells were successively treated with 1 mM hydrogen peroxide (100% oxidation) and 10 mM dithiothreitol (100% reduction). After background correction, the fluorescence emission ratio after excitation at 400 nm (oxidized state) and 480 nm (reduced state) was calculated and the percentage oxidation was determined.

2.5. Determination of GSSG and GSH content in whole-cell homogenates

Preparation of cell extracts and measurement of cellular GSSG and GSH content were performed using HPLC as described previously [44]. Values were expressed as nmol/mg protein.

2.6. Quantification of the extent of lipid peroxidation

Measurement of the extent of lipid peroxidation was performed as described before [40]. Briefly, fibroblasts, grown to ~70% confluence on glass coverslips, were incubated in HEPES–Tris medium containing 4 μM C11-BODIPY[581/591] for 30 min at 37 °C. Upon oxidation, the red emitting form of the dye (595 nm) is converted into a green emitting form (520 nm). After thorough washing, cells were excited at 488 nm and images were collected using the video-rate confocal microscope. Green and red fluorescence emission signals were separated using a 560 DM dichroic mirror and appropriate band-pass filters (535D20 and 580LP; Chroma Technology Corp.). In each experiment, the average of the green to red fluorescence emission ratios obtained with healthy fibroblasts was set at 100%, to which all other values were related.

2.7. Data analysis and statistics

Numerical results were visualized using Origin Pro 7.5 (Originlabs, Northampton, MA, USA) and are expressed as means±S.E. During linear regression analysis, we used Pearson's correlation coefficient R (or product moment correlation coefficient) as an estimate of the population correlation coefficient. R values of -1 and $+1$ indicate a perfect linear correlation between the two variables. For $R>0$ this correlation is positive, whereas for $R<0$ it is negative. During non-linear regression analysis, we used the coefficient of determination (R^2) to express the proportion of the total variation that is explained by the regression. An R^2 value of $+1$ indicates that the total variation in the y-variable can be explained in terms of the regression curve. Statistical

differences between average values were determined using an independent two-population Student's *t*-test (Bonferroni corrected). *p* values <0.05 were considered significant.

2.8. Chemicals

Culture materials and fluorescent probes were obtained from Invitrogen (Breda, The Netherlands). All other reagents were from Sigma (Zwijndrecht, the Netherlands).

3. Results

3.1. Effect of acute rotenone treatment on NAD(P)H autofluorescence in healthy fibroblasts

To investigate whether a decrease in complex I activity can alter the NADH level, we performed video-imaging microscopy of pyridine nucleotide autofluorescence. Because NADPH and NADH have similar spectral properties, an increase in fluorescence intensity reflects *de facto* a net shift in the pyridine nucleotide pool towards the more reduced state [17]. In fibroblasts of a healthy control subject (Table 1; CT1), NAD(P)H autofluorescence mainly originated from elongated tubular structures present in the cytosolic compartment. In previous studies, similar structures were identified as mitochondrial filaments [11,15,40,45]. To have an estimate of the NAD(P)H level in the mitochondrial matrix, we routinely determined its autofluorescence from a circular region of interest harboring a high density of mitochondrial filaments. For background correction, an extracellular region of similar

size was used. Average NAD(P)H autofluorescence remained constant for at least 2 min, but was greatly reduced to $59 \pm 3\%$ of baseline upon short-term treatment with the mitochondrial uncoupler p-trifluoromethoxy carbonyl cyanide phenyl hydrazone (FCCP; 1 μM; 2 min) (Fig. 1A; right bar). In sharp contrast, acute treatment with rotenone (1 μM; 2 min) markedly increased the autofluorescence signal to $149 \pm 9\%$ of baseline (Fig. 1A; middle bar). The effect of rotenone was dose-dependent with half-maximal and maximal inhibitor concentrations of 100 nM and 1 μM, respectively (Fig. 1B, open symbols; $R^2 = 0.93$).

3.2. Relationship between NAD(P)H autofluorescence and HEt oxidation in healthy fibroblasts acutely treated with rotenone

Next, we evaluated the effect of acute inhibition of complex I on the oxidation rate of hydroethidine (HEt) as a putative measure of the intracellular superoxide level. Fibroblasts were incubated with 10 μM HEt and the indicated concentration of rotenone for 10 min, thoroughly washed to remove non-oxidized HEt, and subsequently imaged for quantification of the fluorescent HEt oxidation products formed during the 10-min incubation period with HEt. Importantly, we showed before that the average fluorescence intensity remained stable for at least 10 min, indicating that non-oxidized HEt was effectively removed during the washing step and that its oxidation products did not translocate during the ensuing recording period [15,40]. In addition, we demonstrated that these products accumulated in elongated tubular structures similar to those observed in
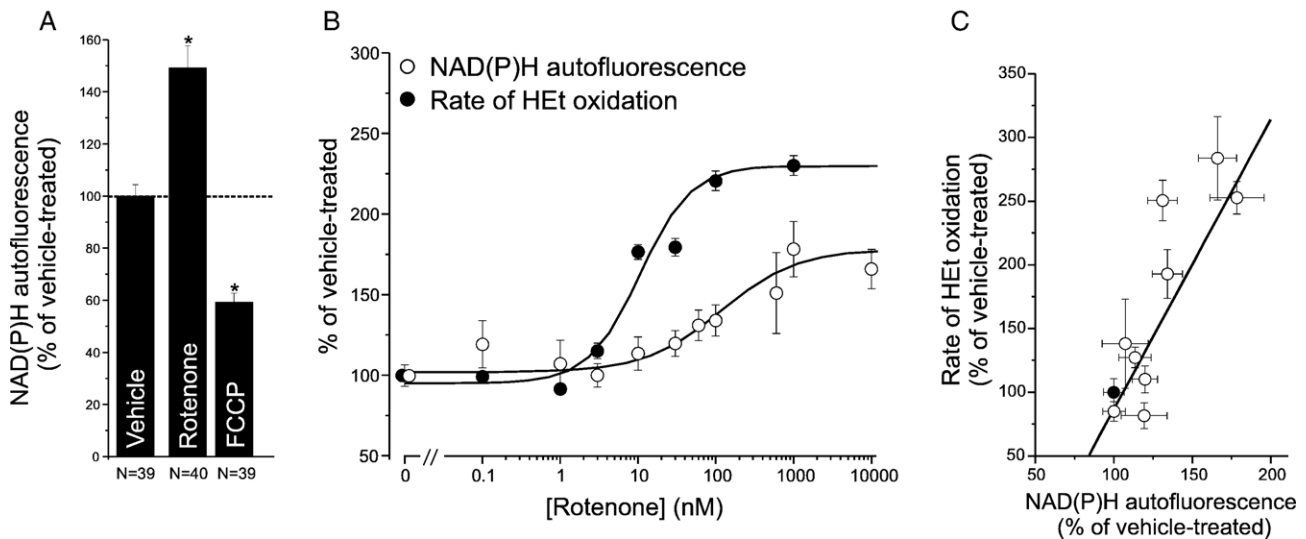

Fig. 1. Acute rotenone treatment increases NAD(P)H autofluorescence and HEt oxidation rate in healthy fibroblasts. (A) CT1 cells (Table 1) were treated with either FCCP (1 μM) or rotenone (1 μM) for 2 min and subsequently monitored for NAD(P)H autofluorescence by video-imaging microscopy. For each cell, the average fluorescence pixel intensity was calculated for a mitochondria-rich region as a measure of the local NAD(P)H level. On each measuring day, the average value obtained with vehicle-treated CT1 cells was set at 100%, to which all values were related. Numerals represent the number of individual cells analysed on at least 3 days. *Significantly different from vehicle-treated control (*p*<0.05). (B) Dose–response curve for the effect of acute rotenone treatment on NAD(P)H autofluorescence (open symbols) and accumulation of hydroethidine (HEt) oxidation products (closed symbols). In the latter case, cells were incubated with 10 μM HEt and the indicated concentration of rotenone for 10 min, thoroughly washed to remove non-oxidized dye and subsequently subjected to video-imaging microscopy. The average fluorescence pixel intensity was calculated for a mitochondria-rich region as a measure of the local superoxide level. The effect of each rotenone concentration was measured on at least three days and expressed relative to the average fluorescence intensity obtained with vehicle-treated CT1 cells measured on the same day. (C) Positive linear correlation between NAD(P)H autofluorescence and HEt oxidation rate in rotenone-treated CT1 cells (data are from panel B).

NAD(P)H autofluorescence measurements. Acute application of rotenone dose-dependently increased the rate of HEt oxidation in a mitochondria-rich region of interest (Fig. 1B, closed symbols; $R^2 = 0.95$). Half-maximal and maximal inhibitor concentrations were 10 nM and 100 nM, respectively. Linear regression analysis revealed a positive correlation between HEt oxidation rate and NAD(P)H autofluorescence for the whole range of rotenone concentrations (Fig. 1C; $R = 0.84$, $p = 0.002$).

3.3. Relationship between NAD(P)H autofluorescence and residual complex I activity in patient fibroblasts

Fibroblasts of complex I deficient patients displayed a similar density of mitochondrial filaments in the perinuclear region as healthy fibroblasts. Measurement of the average NAD(P)H autofluorescence in this mitochondria-rich region showed a significant increase in all but one of the patient cell lines (P9; Table 1). Linear regression analysis revealed a negative correlation between NAD(P)H autofluorescence and residual complex I activity for the whole cohort of patient cell lines (Fig. 2A; $R = -0.87$; $p < 0.001$).

3.4. Relationship between NAD(P)H autofluorescence and HEt and CM-H2DCF oxidation in patient fibroblasts

All but one of the patient cell lines (P2; Table 1) were reported before to display significantly increased rates of HEt and CM-H$_2$DCF oxidation as putative measures of the intracellular levels of superoxide [15,16] and derived ROS [16,41], respectively. Similar as in healthy fibroblasts acutely treated with rotenone, NAD(P)H autofluorescence and HEt oxidation rate were positively correlated for the whole cohort of patient cell lines (Fig. 2B; $R = 0.81$, $p < 0.001$). Likewise,

linear regression analysis revealed a positive correlation between NAD(P)H autofluorescence and CM-H$_2$DCF oxidation rate (Fig. 2C; $R = 0.86$; $p < 0.001$).

3.5. Total cellular glutathione content and GSSG to GSH ratio in patient fibroblasts

The results obtained thus far are in agreement with the idea that the large majority of patient cell lines exhibit a marked increase in NADH level and superoxide and derived ROS levels. This leaves the question of whether and, if so, how the cellular redox environment is altered under these conditions. Evidence has been provided that the ratio between GSH and its oxidized form (GSSG) serves as a major determinant of the cell's redox environment [31]. To establish whether complex I deficiency affects the redox state of this couple, we determined the GSSG and GSH content in whole-cell homogenates of 10 healthy and 10 patient fibroblast cell lines using high performance liquid chromatography. Table 2 shows that on average neither the GSSG nor GSH content differed significantly between fibroblasts of healthy subjects and complex I deficient patients (p values of 0.55 and 0.36, respectively). Similarly, the ratio of GSSG to GSH did not differ between healthy and patient fibroblasts ($p = 0.13$).

3.6. Determination of the subcellular thiol redox state using organelle-targeted roGFP1

To investigate the possibility that the subcellular redox environment is altered in human complex I deficiency, healthy and patient fibroblasts were transduced with recombinant baculoviruses containing the DNA for roGFP1, a redox-sensitive variant of the green fluorescent protein. RoGFP1 was either expressed in the cytosol (cyt-roGFP1) or targeted exclusively to
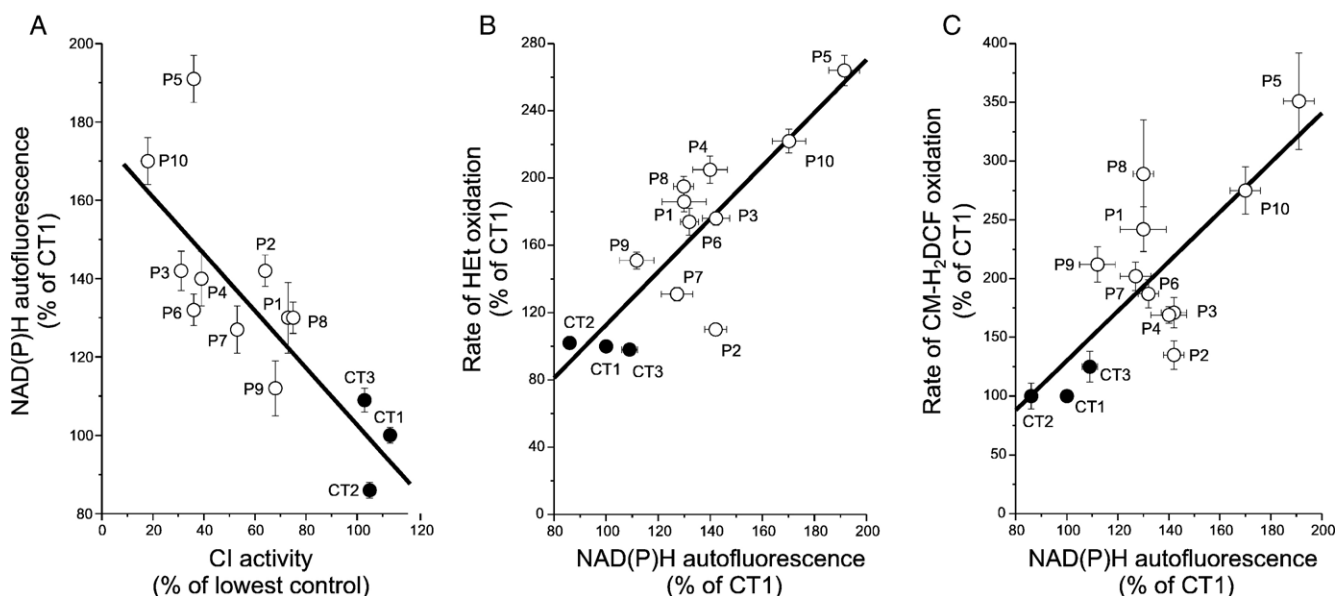

Fig. 2. Correlation between NAD(P)H autofluorescence, residual complex I activity and rates of HEt and CM-H2DCF oxidation in patient fibroblasts. (A) Negative linear correlation between residual complex I activity and NAD(P)H autofluorescence. (B) Positive linear correlation between NAD(P)H autofluorescence and HEt oxidation rate. (C) Positive linear correlation between NAD(P)H autofluorescence and rate of CM-H2DCF oxidation (see Results for details).

Table 2
Cellular thiol redox status

Cell line [a]	mit-roGFP1 [b]	cyt-roGFP1 [b]	GSH+GSSG [c]	GSSG [c] (oxidized)	GSH [c] (reduced)	GSSG/GSH
Average CT	44.6±2.16	17.6±1.25	26.9±1.8	0.793±0.033	26.1±1.8	0.031±0.0020
CT1 (#5120)	38±2 ($n=42$)	15±1 ($n=23$)	25.1	0.911	24.2	0.038
CT2 (#5119)	48±4 ($n=24$)	20±3 ($n=14$)	25.4	0.722	24.7	0.029
CT3 (#5118)	44±4 ($n=22$)	14±2 ($n=11$)	28.0	0.831	27.1	0.031
CT4 (#4996)	39±4 ($n=21$)	20±2 ($n=8$)	25.7	0.805	24.9	0.032
CT5 (#223V)	45±4 ($n=18$)	18±4 ($n=11$)	25.6	0.748	24.9	0.030
CT6 (#MW21)	49±4 ($n=23$)	19±3 ($n=18$)	31.2	0.946	30.3	0.031
CT7 (#MW25)	59±4 ($n=15$)	25±1 ($n=12$)	26.9	0.749	26.2	0.029
CT8 (#MW28)	40±5 ($n=11$)	19±3 ($n=6$)	36.3	0.861	35.5	0.024
CT9 (#MW33)	48±7 ($n=11$)	15±4 ($n=3$)	30.8	0.782	30.0	0.026
CT10 (#MW35)	36±6 ($n=9$)	11±1 ($n=10$)	14.1	0.577	13.5	0.043
Average P	43.3±2.05	21.5±1.40	24.8±1.4	0.830±0.050	24±1.4	0.035±0.0010
P1 (#5171)	40±3 ($n=20$)	19±3 ($n=23$)	29.2	1.014	28.2	0.036
P2 (#5866)	44±4 ($n=23$)	15±1 ($n=13$)	21.6	0.742	20.9	0.036
P3 (#6173)	49±5 ($n=14$)	20±2 ($n=12$)	23.0	0.904	22.1	0.041
P4 (#5170)	44±5 ($n=19$)	18±2 ($n=14$)	27.9	0.783	27.1	0.029
P5 (#5067)	36±3 ($n=21$)	27±2 ($n=21$)	31.7	0.986	30.7	0.032
P6 (#5260)	52±4 ($n=22$)	26±2 ($n=13$)	19.4	0.587	18.8	0.031
P7 (#5737)	54±3 ($n=44$)	26±2 ($n=31$)	19.7	0.732	19.0	0.039
P8 (#4608)	40±3 ($n=28$)	24±3 ($n=15$)	24.3	0.902	23.4	0.039
P9 (#5175)	37±3 ($n=20$)	16±1 ($n=22$)	21.9	0.630	21.3	0.030
P10 (#6603)	37±3 ($n=34$)	24±2 ($n=29$)	29.5	1.017	28.5	0.036

[a] Numbers indicate the designation of the cell lines within the Nijmegen Centre for Mitochondrial Disorders (NCMD). CT and P indicate control and patient cell lines, respectively.

[b] Data reflects the % of oxidized roGFP1 in the mitochondrion (mit-roGFP1) and cytosol (cyt-roGFP1); values between brackets represent the number of individual cells analyzed on at least 4 days.

[c] Expressed as nmol/mg protein, determined in two independent experiments.

the mitochondrial matrix (mit-roGFP1). Both proteins were readily expressed and their fluorescence was determined in circular regions marked 'm' (Fig. 3A) and 'c' (Fig. 3B), respectively. For background correction, an extracellular region of similar size (marked 'b') was used. Fig. 1C depicts the ratio of the fluorescence emission intensities after excitation at 400 and 480 nm as a function of time. To establish the extent of roGFP1 oxidation, ratio signals were calibrated by successive treatment with 1 mM hydrogen peroxide (H_2O_2) and 10 mM dithiothreitol (DTT) to fully oxidize (100% oxidation) and reduce (0% oxidation) the probe, respectively [43]. H_2O_2 gradually increased the fluorescence emission ratio to a maximum reached within 350 s, whereas subsequent addition of DTT rapidly reduced this ratio to below pre-H_2O_2 levels. Higher concentrations of H_2O_2 and DTT caused no further change in fluorescence emission ratio, indicating that the probe was maximally oxidized and reduced, respectively. Fig. 3C shows that for healthy fibroblasts (Table 1; CT1), the extent of roGFP1 oxidation was higher in the mitochondrial matrix than in the cytosol.

3.7. Effect of GSH depletion on the subcellular thiol redox state in healthy fibroblasts

To assess the relevance of the GSSG/GSH couple in preserving the subcellular redox environment, healthy fibroblasts were cultured in the presence of 12.5 μM L-buthionine-(S,R)-sulphoximine (BSO) for 72 h. BSO is a potent inhibitor of γ-glutamylcysteine synthetase, the rate limiting enzyme in the synthesis of GSH [46], and it has been demonstrated that chronic treatment with this drug effectively depletes GSH

[47,48]. BSO dramatically increased the extent of roGFP1 oxidation in both mitochondrial matrix (Fig. 3D) and cytosolic compartment (Fig. 3E). Moreover, this inhibitor caused a marked decrease in the rate of HEt oxidation (Fig. 3F), whereas, in sharp contrast, it substantially increased the rate of CM-H_2DCF oxidation (Fig. 3G). Moreover, it slightly increased NAD(P)H autofluorescence (Fig. 3H).

3.8. Effect of chronic rotenone treatment on the subcellular thiol redox state in healthy fibroblasts

We previously showed that chronic rotenone treatment dose-dependently reduced the activity of complex I in healthy fibroblasts [40]. To determine whether complex I deficiency could, in principle, alter the subcellular redox environment, healthy fibroblasts (Table 1; CT1) were treated with 100 nM rotenone for 72 h. This treatment slightly but significantly ($p<0.05$) increased the extent of mit-roGFP1 and cyt-roGFP1 oxidation (Fig. 3D and E, respectively). Experiments performed in parallel confirmed previous work [15] showing that chronic rotenone treatment increased the rate of HEt oxidation (Fig. 3F). Surprisingly, this treatment did not alter the rate of CM-H_2DCF oxidation (Fig. 3G), whereas it markedly increased NAD(P)H autofluorescence (Fig. 3H).

3.9. Measurement of the subcellular thiol redox state in patient fibroblasts

To establish whether complex I deficiency is associated with a change in subcellular redox environment, fibroblasts of 10
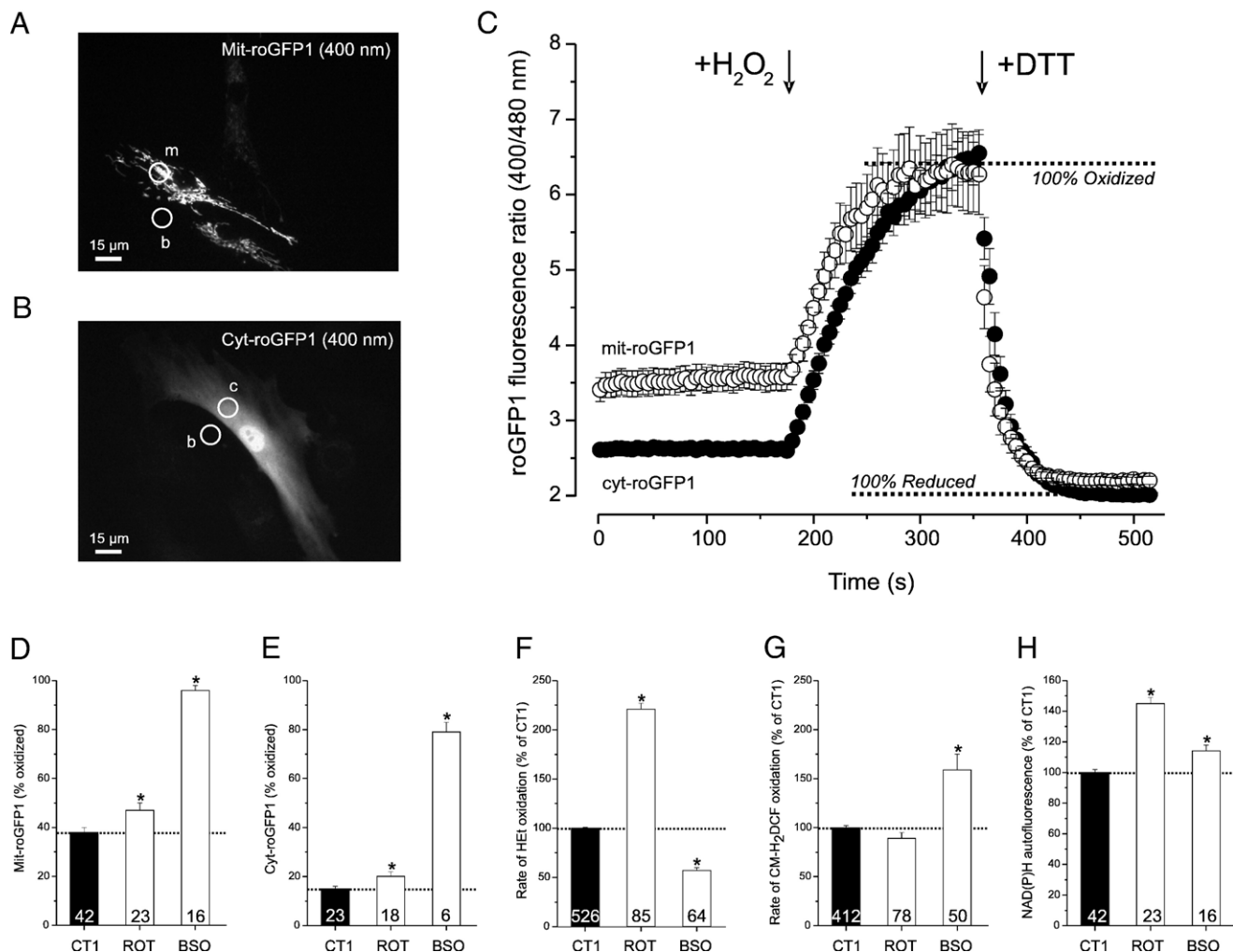
Fig. 3. Quantitative measurement of subcellular thiol redox state with roGFP1. (A) Fluorescence image (400 nm excitation) of a healthy fibroblast (Table 1; CT1) transiently expressing the mitochondria-targeted variant of roGFP (mito-roGFP1). (B) The same following transient expression of the cytosolic variant of roGFP1 (cyt-roGFP1). Circles represent regions of interest used for quantitative measurement of thiol redox state in the mitochondrial matrix (m), the cytosolic compartment (c) and an extracellular region used for background correction (b). (C) Quantification of the subcellular thiol redox state using 1 mM H_2O_2 (maximal oxidation) and 10 mM DTT (maximal reduction). After background correction, the 400/480 nm fluorescence excitation intensity was calculated. Note that roGFP1 is more oxidized in the mitochondrial matrix. (D, E) CT1 fibroblasts, transiently expressing organelle-targeted roGFP, were treated with either rotenone (100 nM) or BSO (12.5 μM) for 72 h and used for analysis of the thiol redox state in the (D) mitochondrial matrix and (E) cytosolic compartment as described above. (F–H) CT1 cells, chronically treated with either rotenone or BSO, were subjected to video-imaging microscopy for quantification of the rates of (F) HEt oxidation and (G) CM-H_2DCF oxidation and (H) NAD(P)H autofluorescence as described in the legend to Fig. 1. On each day, the average value obtained with vehicle-treated CT1 cells was set at 100%, to which all values were related. Numerals indicate the number of cells analyzed on at least 3 days. *Significantly different from vehicle-treated control ($p < 0.05$).

healthy subjects and 10 patients were transduced with mit-roGFP1 and cyt-roGFP1 and analyzed as described above. In all cases, mit-roGFP1 was significantly more oxidized than cyt-roGFP1 (Table 2). Unexpectedly, however, no significant differences in mitochondrial and/or cytosolic roGFP1 oxidation were observed between healthy and complex I deficient cell lines.

3.10. Measurement of lipid peroxidation in patient fibroblasts

We previously showed that chronic rotenone treatment (100 nM, 72 h) significantly increased the extent of lipid peroxidation in healthy fibroblasts and that this effect of the inhibitor was abolished by the mitochondria-targeted antioxidant mitoquinone [40]. Here, we used the same measuring protocol but could not detect any difference in the extent of lipid peroxidation between patient cell lines and cell lines of healthy subjects (Table 1).

4. Discussion

In this study, we measured the thiol redox state as an important determinant of the redox environment in both the cytosol and mitochondrial matrix of cultured skin fibroblasts of 10 healthy control subjects and 10 patients with nuclear-inherited isolated complex I deficiency. In addition to previously reported increases in oxidation rates of hydroethidine (HEt) and CM-H_2DCF as putative measures of intracellular superoxide [15,16] and derived ROS [16,41] levels, respectively, we here show that NAD(P)H autofluorescence is increased in a mito-

chondria-rich region, which is compatible with a rise in mitochondrial NADH level. Strikingly, however, neither the thiol redox state nor the extent of lipid peroxidation differed significantly between the healthy and patient cell lines.

4.1. HEt and CM-H$_2$DCF are primarily oxidized by different ROS

Studies with isolated mitochondria have indicated that OXPHOS-derived superoxide is predominantly released into the mitochondrial matrix, where it is rapidly converted into hydrogen peroxide (H$_2$O$_2$) [49]. The mitochondrial matrix is devoid of catalase and uses glutathione peroxidase (GPX) to fully reduce H$_2$O$_2$ into water. Reducing equivalents are obtained from glutathione (GSH), which is oxidized to glutathione disulfide (GSSG) [50]. We showed before that exogenous H$_2$O$_2$ readily increased the rate of CM-H$_2$DCF oxidation, without altering the rate of HEt oxidation [40]. Here, we show that chronic BSO treatment increased the rate of CM-H$_2$DCF oxidation, whereas, at the same time, it decreased the rate of HEt oxidation, indicating that the ROS that oxidize CM-H$_2$DCF do not oxidize HEt. On the other hand, chronic rotenone treatment increased the rate of HEt oxidation, whereas, at the same time, it did not alter the rate of CM-DCF formation. These findings are compatible with the idea that HEt is mainly oxidized by superoxide, whereas CM-H$_2$DCF is predominantly oxidized by superoxide-derived ROS. Because the formation of fluorescent oxidation products occurred linearly with time, the rate of fluorescence increase, then, is a measure of the superoxide and derived ROS level, respectively.

4.2. Cellular NAD(P)H levels are increased in nuclear-inherited complex I deficiency

The present study reveals that steady-state NAD(P)H levels are increased in virtually all patient cell lines with biochemically diagnosed complex I deficiency. A negative linear correlation was found between NAD(P)H autofluorescence and complex I-specific NADH oxidizing capacity, suggesting that the observed increase in NAD(P)H autofluorescence reflects primarily an increase in NADH level. This conclusion was substantiated by the finding that healthy fibroblasts displayed a dose-dependent increase in NAD(P)H autofluorescence following acute inhibition of complex I by rotenone. The present study furthermore reveals a positive linear correlation between NAD(P)H and superoxide levels. The same correlation was observed for healthy fibroblasts acutely treated with rotenone. These results are in agreement with earlier findings [23–27] and support the idea that complex I deficiency increases the fraction of reduced flavin in complex I and, thus, OXPHOS-derived superoxide production [22]. Here it should be noted, however, that the situation might be different in other model systems. For instance, using isolated guinea pig hearts it was found that the complex I inhibitor amobarbital attenuated the increase in HEt oxidation but not the increase in NAD(P)H autofluorescence during 30 min of ischemia [51].

4.3. Cellular redox environment is not detectably altered in nuclear-inherited complex I deficiency

It has been suggested that the redox state of roGFP1 is determined by the reducing capacity of the most important redox buffer within the cell [42]. Here, we show that inhibition of GSH synthesis by L-buthionine-(S,R)-sulphoximine (BSO) resulted in virtually complete oxidation of both mit- and cyt-roGFP1. This result indicates that the GSSG/GSH redox couple is the most important determinant of the subcellular redox environment in human skin fibroblasts. ROS despite a marked increase in the intracellular levels of superoxide and derived ROS, the total cellular GSH content and the GSSG to GSH ratio were not detectably altered in a large cohort of patient cell lines. In agreement with this result, measurements with roGFP1 revealed no significant differences in thiol redox state between patient and healthy fibroblasts. A similar lack of effect of increased ROS levels on the oxidation state of roGFP1 was observed in EGF-treated NR6 cells [42]. Our results disagree with a recent study showing a decrease in total cellular glutathione content in patient fibroblasts with a mutation in the *NDUFS1* gene [14]. However, the latter study included only one healthy control cell line and we show here that the total cellular glutathione content varied over the same range in both the patient and healthy control group. In agreement with our results, the total cellular glutathione content was previously found to be unaltered in patient fibroblasts with a mutation in the *NDUFS4* gene [14].

Taken together, our findings show that patient fibroblasts are able to maintain the thiol redox state and, consequently, the cellular redox environment, despite marked increases in superoxide and derived ROS levels. Because GSSG, produced by the action of GPX, is reconverted to GSH by enzymes that use NADPH as electron donor [52] and NAD(P)H levels are increased in patient fibroblasts, it may be speculated that the absence of any detectable change in cellular redox environment is due to the increased action of these enzymes. As far as the mitochondrial matrix is concerned, evidence has been provided that NADP$^+$-dependent isocitrate dehydrogenase is a major producer of mitochondrial NADPH [53], whereas, in addition, NADH can be converted into NADPH by the action of mitochondrial transhydrogenase [54].

In both healthy and patient fibroblasts mit-roGFP1 (values of 45% and 43%, respectively) was significantly more oxidized than cyt-roGFP1 (values of 18% and 22%, respectively). Similar results were obtained with HeLa cells (values of 33% and 18%, respectively; [42,43]). The finding that the redox environment is more oxidized in the mitochondrial matrix is in accordance with the observation that the large majority of cellular ROS is produced as a consequence of oxidative phosphorylation [17,18,49,55].

BSO slightly increased the NAD(P)H level, suggesting that the mitochondrial redox environment is a determinant of OXPHOS function. In agreement with this conclusion, oxidation of the mitochondrial GSH pool was found to reduce the activity of complex I [56]. Furthermore, BSO decreased the superoxide level, whereas, at the same time, it markedly increased the

cytosolic ROS level, demonstrating the importance of GPX in scavenging superoxide-derived ROS. The latter two findings are in agreement with the recent observation that BSO increases the expression of superoxide dismutases [57,58].

Our results with BSO and rotenone show that the absence of any detectable alteration in subcellular thiol redox state is not due to a lack of sensitivity of roGFP1 because BSO almost completely oxidized this sensor, whereas rotenone, at a concentration shown before to inhibit the activity of complex I by ~80% [40], only slightly increased the amount of oxidized roGFP1. The results obtained with this inhibitor substantiate our conclusion that complex I deficiency only slightly, if at all, oxidizes the subcellular redox environment in human skin fibroblasts. As speculated above, this finding may be explained by the rotenone-induced increase in NAD(P)H level, resulting in the increased action of enzymes that use NADPH to regenerate GSH. An efficient regeneration of GSH may also explain the inability of chronic rotenone to increase the intracellular level of superoxide-derived ROS, because it allows adequate detoxification of H_2O_2 by GPX. In agreement with this explanation, chronic rotenone caused a significant but small increase in the fraction of oxidized roGFP1 in both mitochondrial matrix and cytosolic compartment.

4.4. Lipid peroxidation is not detectably altered in inherited complex I deficiency

When the production of oxidants exceeds the antioxidant capacity of the cell, this may cause damage to lipids, proteins and DNA. Importantly, the extent of damage to a particular target depends, among others, on the type of oxidant involved, the location of the target versus the oxidant, the oxidant to target ratio and the occurrence of repair reactions. It has been demonstrated that inadequate detoxification of H_2O_2 may result in the formation of highly reactive hydroxyl radicals through the classic Fe^{2+}-catalyzed Fenton reaction. As far as human complex I deficiency is concerned, experimental evidence suggests that this condition may indeed lead to an increased production of this radical and consequent increase in the extent of lipid peroxidation [20]. In accordance with these results, we demonstrated that chronic treatment with rotenone caused a 2-fold increase in the extent of lipid peroxidation [40]. Contradictory to these results, however, we now show that the extent of lipid peroxidation is not detectably altered in patient fibroblasts. Together with our conclusion that the GSSG/GSH couple is the most important determinant of the cellular redox environment and our finding that the redox state of this couple is not detectably altered in patient fibroblasts, this finding is compatible with previous conclusions that the presence of sufficient amounts of GSH can prevent the occurrence of oxidant-induced damage [59].

Acknowledgements

References

[1] J.A.M. Smeitink, L.W.P.J. van den Heuvel, S. DiMauro, The genetics and pathology of oxidative phosphorylation, Nat. Rev., Genet. 2 (2001) 342–352.

[2] J. Carroll, I.M. Fearnley, R.J. Shannon, J. Hirst, J.E. Walker, Analysis of the subunit composition of complex I from bovine heart mitochondria, Mol. Cell. Proteomics 2 (2003) 117–126.

[3] J. Carroll, I.M. Fearnley, J.M. Skehel, R.J. Shannon, J. Hirst, J.E. Walker, Bovine complex I is a complex of forty-five different subunits, J. Biol. Chem. 281 (2006) 32724–32727.

[4] T. Gabaldon, D. Rainey, M.A. Huynen, Tracing the evolution of a large protein complex in the eukaryotes, NADH:ubiquinone oxidoreductase (Complex I), J. Mol. Biol. 348 (2005) 857–870.

[5] S.M. Budde, L.W.P.J. van den Heuvel, R.J. Smeets, D. Skladal, J.A. Mayr, C. Boelen, V. Petruzzella, S. Papa, J.A.M. Smeitink, Clinical heterogeneity in patients with mutations in the NDUFS4 gene of mitochondrial complex I, J. Inherit. Metab. Dis. 26 (2003) 813–815.

[6] P. Benit, A. Slama, F. Cartault, I. Giurgea, D. Chretien, S. Lebon, C. Marsac, A. Munnich, A. Rotig, P. Rustin, P, Mutant NDUFS3 subunit of mitochondrial complex I causes Leigh syndrome, J. Med. Genet. 41 (2004) 14–17.

[7] R.J. Janssen, L.W.P.J. van den Heuvel, J.A.M. Smeitink, Genetic defects in the oxidative phosphorylation (OXPHOS) system, Expert Rev. Mol. Diagn. 4 (2004) 143–156.

[8] D.M. Kirby, R. Salemi, C. Sugiana, A. Ohtake, L. Parry, K.M. Bell, E.P. Kirk, A. Boneh, R.W. Taylor, H.H. Dahl, M.T. Ryan, D.R. Thorburn, NDUFS6 mutations are a novel cause of lethal neonatal mitochondrial complex I deficiency, J. Clin. Invest. 114 (2004) 837–845.

[9] I. Ogilvie, N.G. Kennaway, E.A. Shoubridge, A molecular chaperone for mitochondrial complex I assembly is mutated in a progressive encephalopathy, J. Clin. Invest. 115 (2005) 2784–2792.

[10] C. Ugalde, R.J.R.J. Janssen, L.W.P.J. van den Heuvel, J.A.M. Smeitink, L.G.J. Nijtmans, Differences in assembly or stability of complex I and other mitochondrial OXPHOS complexes in inherited complex I deficiency, Hum. Mol. Genet. 13 (2004) 659–667.

[11] W.J.H. Koopman, H.J. Visch, S. Verkaart, L.W.P.J. van den Heuvel, J.A.M. Smeitink, P.H.G.M. Willems, Mitochondrial network complexity and pathological decrease in complex I activity are tightly correlated in isolated human complex I deficiency, Am. J. Physiol.: Cell Physiol. 289 (2005) C881–C890.

[12] H.J. Visch, G.A. Rutter, W.J.H. Koopman, J.B. Koenderink, S. Verkaart, T. de Groot, A. Varadi, K.J. Mitchell, L.W.P.J. van den Heuvel, J.A.M. Smeitink, P.H.G.M. Willems, Inhibition of mitochondrial Na^+–$Ca2^+$ exchange restores agonist-induced ATP production and $Ca2^+$ handling in human complex I deficiency, J. Biol. Chem. 279 (2004) 40328–40336.

[13] H.J. Visch, W.J.H. Koopman, A. Leusink, S.E. van Emst-de Vries, L.W.P.J. van den Heuvel, P.H.G.M. Willems, J.A.M. Smeitink, Decreased agonist-stimulated mitochondrial ATP production caused by a pathological reduction in endoplasmic reticulum calcium content in human complex I deficiency, Biochim. Biophys. Acta 1762 (2006) 115–123.

[14] A. Iuso, S. Scacco, C. Piccoli, F. Bellomo, V. Petruzzella, R. Trentadue, M. Minuto, M. Ripoli, N. Capitanio, M. Zeviani, S. Papa, Dysfunctions of

cellular oxidative metabolism in patients with mutations in the NDUFS1 and NDUFS4 genes of complex I, J. Biol. Chem. 281 (2006) 10374–10380.

[15] S. Verkaart, W.J.H. Koopman, S.E. van Emst-de Vries, L.G.J. Nijtmans, L.W.P.J. van den Heuvel, J.A.M. Smeitink, P.H.G.M. Willems, Superoxide production is inversely related to complex I activity in inherited complex I deficiency, Biochim. Biophys. Acta 1772 (2007) 373–381.

[16] W.J.H. Koopman, S. Verkaart, H.J. Visch, S.E. van Emst-de Vries, L.G.J. Nijtmans, J.A.M. Smeitink, P.H.G.M. Willems, Human NADH:ubiquinone oxidoreductase deficiency: radical changes in mitochondrial morphology? Am. J. Physiol.: Cell Physiol. Apr. 11 (2007). PMID: 1728841.

[17] M.R. Duchen, Mitochondria in health and disease: perspectives on a new mitochondrial biology, Mol. Aspects Med. 25 (2004) 365–451.

[18] R.S. Balaban, S. Nemoto, T. Finkel, Mitochondria, oxidants, and aging, Cell 120 (2005) 483–495.

[19] H.J. Forman, J.M. Fukuto, M. Torres, Redox signaling: thiol chemistry defines which reactive oxygen and nitrogen species can act as second messengers, Am. J. Physiol.: Cell Physiol. 287 (2004) C246–C256.

[20] X. Luo, S. Pitkänen, S. Kassovska-Bratinova, B.H. Robinson, D.C. Lehotay, Excessive formation of hydroxyl radicals and aldehydic lipid peroxidation products in cultured skin fibroblasts from patients with complex I deficiency, J. Clin. Invest. 99 (1997) 2877–2882.

[21] D. Giustarini, R. Rossi, A. Milzani, R. Colombo, I. Dalle-Donne, S-gluta-thionylation: from redox regulation of protein functions to human diseases, J. Cell. Mol. Med. 8 (2004) 201–212.

[22] L. Kussmaul, J. Hirst, The mechanism of superoxide production by NADH:ubiquinone oxidoreductase (complex I) from bovine heart mitochondria, Proc. Natl. Acad. Sci. U. S. A. 103 (2006) 7607–7612.

[23] R.G. Hansford, B.A. Hogue, V. Mildaziene, Dependence of H_2O_2 formation by rat heart mitochondria on substrate availability and donor age, J. Bioenerg. Biomembr. 29 (1997) 89–95.

[24] Y. Liu, G. Fiskum, D. Schubert, Generation of reactive oxygen species by the mitochondrial electron transport chain, J. Neurochem. 80 (2002) 780–787.

[25] Y. Kushnareva, A.N. Murphy, A. Andreyev, Complex I-mediated reactive oxygen species generation: modulation by cytochrome c and NAD(P)$^+$ oxidation–reduction state, Biochem. J. 368 (2002) 545–553.

[26] A.P. Kudin, N.Y.-B. Bimpong-Buta, S. Vielhaber, W.S. Kunz, Characterization of superoxide-producing sites in isolated brain mitochondria, J. Biol. Chem. 279 (2004) 4127–4135.

[27] A.A. Starkov, G. Fiskum, Regulation of brain mitochondrial H_2O_2 production by membrane potential and NAD(P)H redox state, J. Neurochem. 86 (2003) 1101–1107.

[28] S. Raha, B.H. Robinson, Mitochondria, oxygen free radicals, and apoptosis, Am. J. Med. Genet. 106 (2001) 62–70.

[29] A.M. James, H.M. Cocheme, M.P. Murphy, Mitochondria-targeted redox probes as tools in the study of oxidative damage and ageing, Mech. Ageing Dev. 126 (2005) 982–986.

[30] H. Liu, R. Colavitti, I.I. Roira, T. Finkel, Redox-dependent transcriptional regulation, Circ. Res. 97 (2005) 967–974.

[31] F.Q. Schafer, G.R. Buettner, Redox environment of the cell as viewed through the redox state of the glutathione disulfide/glutathione couple, Free Radical Biol. Med. 30 (2001) 1191–1212.

[32] G. Wu, Y.Z. Fang, S. Yang, J.R. Lupton, N.D. Turner, Glutathione metabolism and its implications for health, J. Nutr. 134 (2004) 489–492.

[33] T.R. Hurd, A. Filipovska, N.J. Costa, C.C. Dahm, M.P. Murphy, Disulphide formation on mitochondrial protein thiols, Biochem. Soc. Trans. 33 (2005) 1390–1393.

[34] H. Raza, M.A. Robin, J.K. Fang, N.G. Avadhani, Multiple isoforms of mitochondrial glutathione S-transferases and their differential induction under oxidative stress, Biochem. J. 366 (2002) 45–55.

[35] O.W. Griffith, A. Meister, Origin and turnover of mitochondrial glutathione, Proc. Natl. Acad. Sci. U. S. A. 82 (1985) 4668–4672.

[36] A. Colell, C. Garcia-Ruiz, M. Miranda, E. Ardite, M. Mari, A. Morales, F. Corrales, N. Kaplowitz, J.C. Fernandez-Checa, Selective glutathione depletion of mitochondria by ethanol sensitizes hepatocytes to tumor necrosis factor, Gastroenterology 115 (1998) 1541–1551.

[37] U. Wullner, J. Seyfried, P. Groscurth, S. Beinroth, S. Winter, M. Gleichmann, M. Heneka, P. Loschmann, J.B. Schulz, M. Weller, T. Klockgether, Glutathione depletion and neuronal cell death: the role of reactive oxygen intermediates and mitochondrial function, Brain Res. 826 (1999) 53–62.

[38] H. Muyderman, M. Nilsson, N.R. Sims, Highly selective and prolonged depletion of mitochondrial glutathione in astrocytes markedly increases sensitivity to peroxynitrite, J. Neurosci. 24 (2004) 8019–8028.

[39] J.A.M. Smeitink, R. Sengers, F. Trijbels, L.W.P.J. van den Heuvel, Human NADH:ubiquinone oxidoreductase, J. Bioenerg. Biomembr. 33 (2001) 259–266.

[40] W.J.H. Koopman, S. Verkaart, H.J. Visch, F.H. van der Westhuizen, M.P. Murphy, L.W.P.J. van den Heuvel, J.A.M. Smeitink, P.H.G.M. Willems, Inhibition of complex I of the electron transport chain causes O_2^--mediated mitochondrial outgrowth, Am. J. Physiol.: Cell Physiol. 288 (2005) C1440–C1450.

[41] W.J.H. Koopman, S. Verkaart, S.E. van Emst-de Vries, S. Grefte, J.A.M. Smeitink, P.H.G.M. Willems, Simultaneous quantification of oxidative stress and cell spreading using 5-(and-6)-chloromethyl-2′,7′-dichloro-fluorescein, Cytometry, A 69 (2006) 1184–1192.

[42] C.T. Dooley, T.M. Dore, G.T. Hanson, W.C. Jackson, S.J. Remington, R.Y. Tsien, Imaging dynamic redox changes in mammalian cells with green fluorescent protein indicators, J. Biol. Chem. 279 (2004) 22284–22293.

[43] G.T. Hanson, R. Aggeler, D. Oglesbee, M. Cannon, R.A. Capaldi, R.Y. Tsien, S.J. Remington, Investigating mitochondrial redox potential with redox-sensitive green fluorescent protein indicators, J. Biol. Chem. 79 (2004) 13044–13053.

[44] A. De Graaf-Hess, F. Trijbels, H. Blom, New method for determining cystine in leukocytes and fibroblasts, Clin. Chem. 45 (1999) 2224–2228.

[45] W.J.H. Koopman, H.J. Visch, J.A.M. Smeitink, P.H.G.M. Willems, Simultaneous quantitative measurement and automated analysis of mitochondrial morphology, mass, potential, and motility in living human skin fibroblasts, Cytometry, A 69 (2006) 1–12.

[46] O.W. Griffith, A. Meister, Potent and specific inhibition of glutathione synthesis by buthionine sulfoximine (S-n-butyl homocysteine sulfoxi-mine), J. Biol. Chem. 254 (1979) 7558–7560.

[47] M.E. Anderson, Glutathione: an overview of biosynthesis and modulation, Chem.-Biol. Interact. 111/112 (1998) 1–14.

[48] T. Fojo, S. Bates, Strategies for reversing drug resistance, Oncogene 22 (2003) 7512–7523.

[49] A.J. Lambert, M.D. Brand, Inhibitors of the quinone-binding site allow rapid superoxide production from mitochondrial NADH:ubiquinone oxidoreductase (Complex I), J. Biol. Chem. 279 (2004) 39414–39420.

[50] R.S. Esworthy, Y.S. Ho, F.F. Chu, The Gpx1 gene encodes mitochondrial glutathione peroxidase in the mouse liver, Arch. Biochem. Biophys. 340 (1997) 59–63.

[51] Q. Chen, A.K.S. Camara, D.F. Stowe, C.L. Hoppel, E.J. Lesnefsky, Modulation of electron transport protects cardiac mitochondria and decreases myocardial injury during ischemia and reperfusion, Am. J. Physiol.: Cell Physiol. 292 (2007) C137–C147.

[52] M.J. Kelner, M.A. Montoya, Structural organization of the human glutathione reductase gene: determination of correct cDNA sequence and identification of a mitochondrial leader sequence, Biochem. Biophys. Res. Commun. 269 (2000) 366–368.

[53] I.S. Kil, J.W. Park, Regulation of mitochondrial NADP$^+$-dependent isocitrate dehydrogenase activity by glutathionylation, J. Biol. Chem. 280 (2005) 10846–10854.

[54] J. Rydström, Mitochondrial transhydrogenase—A key enzyme in insulin secretion and, potentially, diabetes, Trends Biochem. Sci. 31 (2006) 355–358.

[55] F.L. Muller, Y. Liu, H. van Remmen, Complex III releases superoxide to both sides of the inner mitochondrial membrane, J. Biol. Chem. 279 (2004) 49064–49073.

[56] S.M. Beer, E.R. Taylor, S.E. Brown, C.C. Dahm, N.J. Costa, M.J. Runswick, M.P. Murphy, Glutaredoxin 2 catalyzes the reversible oxidation and glutathionylation of mitochondrial membrane thiol proteins: implications for mitochondrial redox regulation, antioxidant defense, J. Biol. Chem. 279 (2004) 47939–47951.

[57] J. Chen, A. Small-Howard, A. Yin, M.J. Berry, The responses of Ht22 cells to oxidative stress induced by buthionine sulfoximine (BSO), BMC Neurosci. 6 (2005) 10.

[58] R.J. Ford, D.A. Graham, S.G. Denniss, J. Quadrilatero, J.W. Rush, Glutathione depletion in vivo enhances contraction and attenuates endothelium-dependent relaxation of isolated rat aorta, Free Radical Biol. Med. 40 (2006) 670–678.

[59] D.L. Hollins, H.B. Suliman, C.A. Piantadosi, M.S. Carraway, Glutathione regulates susceptibility to oxidant-induced mitochondrial DNA damage in human lymphocytes, Free Radical Biol. Med. 40 (2006) 1220–1226.